Z. angew. Math. Phys. 58 (2007) 289–308
0044-2275/07/020289-20
DOI 10.1007/s00033-006-5058-y
© 2006 Birkhäuser Verlag, Basel

Zeitschrift für angewandte Mathematik und Physik ZAMP

On the bidirectional vortex and other similarity solutions in spherical coordinates

Joseph Majdalani* and Sjoerd W. Rienstra

Abstract. The bidirectional vortex refers to the bipolar, coaxial swirling motion that can be triggered, for example, in cyclone separators and some liquid rocket engines with tangential aft-end injectors. In this study, we present an exact solution to describe the corresponding bulk motion in spherical coordinates. To do so, we examine both linear and nonlinear solutions of the momentum and vorticity transport equations in spherical coordinates. The assumption will be that of steady, incompressible, inviscid, rotational, and axisymmetric flow. We further relate the vorticity to some power of the stream function. At the outset, three possible types of similarity solutions are shown to fulfill the momentum equation. While the first type is incapable of satisfying the conditions for the bidirectional vortex, it can be used to accommodate other physical settings such as Hill's vortex. This case is illustrated in the context of inviscid flow over a sphere. The second leads to a closed-form analytical expression that satisfies the boundary conditions for the bidirectional vortex in a straight cylinder. The third type is more general and provides multiple solutions. The spherical bidirectional vortex is derived using separation of variables and the method of variation of parameters. The three-pronged analysis presented here increases our repertoire of general mean flow solutions that rarely appear in spherical geometry. It is hoped that these special forms will permit extending the current approach to other complex fluid motions that are easier to capture using spherical coordinates.

Mathematics Subject Classification (2000). 35D05, 35J05, 35J60, 76B47, 76M23.

Keywords. Vortex flow, cyclone, nonlinear PDE, multiple solutions.

1. Introduction

In the last five decades, considerable attention has been given to naturally occurring swirl patterns in thermal and physical transport applications [1–25]. In that vein, different methods have been employed to simulate and trigger swirl in cylindrical or conical chambers using, for example, tangential fluid injection, inlet swirl vanes, aerodynamically-shaped swirl blades, propellers, vortex trippers, twisted tape inserts, coiled wires, vortex generators, and other swirl-prop devices.

Recently, an efficient cooling method has been proposed by Chiaverini and co-

*Corresponding author: Joseph Majdalani, e-mail: drmajdalani@gmail.com

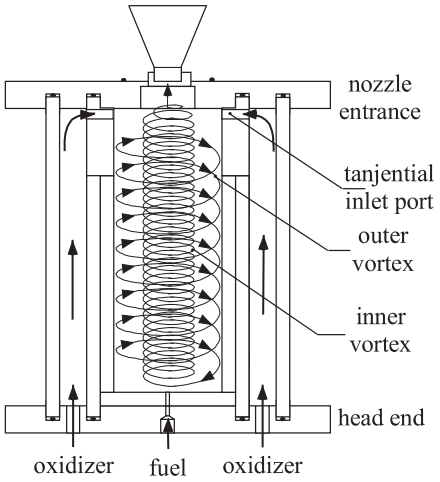

Figure 1. Schematic of the Cool Wall Bidirectional Vortex Combustion Chamber (CWBVCC).

workers [26–28] who have managed to reproduce cyclonic motion inside a liquid rocket engine (see Fig. 1). Their technique is based on inducing a coaxial, co-spinning, bidirectional flow comprising two distinct concentric fields: an outer annular vortex and an inner, tubular vortex. The flow configuration in this chamber is unique in that the oxidizer is injected tangentially into the combustion chamber and just upstream of the nozzle; the process results in a swirling combustion field that exhibits an outer, virtually nonreactive, flow region. This so-called outer vortex fills the annular region separating the combustion core from the chamber's circumferential wall. The combustion core is formed from the oxidizer mixing and reacting with the fuel. The latter is injected radially or axially at the chamber head end. Before reaching the fuel injector's faceplate, the outer vortex (composed of cool oxidizer) coils around and up the chamber wall. The engendered thermal blanket protects the chamber wall from fluctuating heating loads. The attendant lowering of wall temperatures is sufficiently efficient to the extent that a laboratory test using a fuel-rich Hydrogen-Oxygen combustion could be safely sustained in a Plexiglas model of this engine [26–28]. The thermal protection feature not only reduces cooling requirements but leads to appreciable cost reduction, prolonged life, more flexibility in material selection, and reduced weight. The inner vortex, on the other hand, plays an important role in improving combustion efficiency. The inherent swirl increases fuel residence time, mixing, and turbulence, thus improving overall efficiency and ballistic performance. The spinning vortices provide an extended flow path that exceeds the geometric length of the chamber, thus taking full advantage of the chamber's volumetric capacity.

The utilization of bidirectional vortex motion is, in fact, a well established technology that dates back to the 1950s. The earliest investigations may be credited

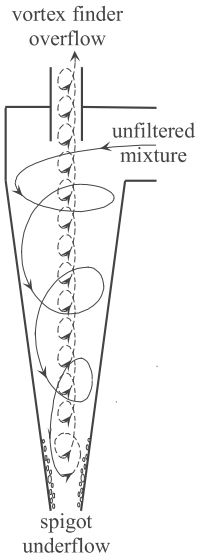

Figure 2. Schematic of a conical separator depicting its key components.

to the experimental work of ter Linden [1] on dust separators and the treatment of hydraulic and gas cyclones by Kelsall [2] and Smith [3, 4]. Theoretical analyses have also been carried out by Fontein and Dijksman [5], Smith [3, 4], and Bloor and Ingham [6–8]. Semi-empirical models are, in turn, available from Reydon and Gauvin [9], Vatistas, Lin and Kwok [10, 11], Vatistas [12], and others. In view of continual progress in computational mechanics, numerical simulations have been recently undertaken by Hsieh and Rajamani [13], Hoekstra, Derksen and Van den Akker [14], Derksen and Van den Akker [15], and Fang, Majdalani and Chiaverini [16].

Generally, cyclone technology is implemented in coal gas purificators, spray dryers, oil-water separators, gas scrubbers, gas dedustors, hydrocyclones, and magneto-hydrodynamic gas core nuclear rockets. Some are widely used in the petrochemical and powder processing industries where they are employed in catalyst or product recovery, scrubbing, and dedusting. The typical cyclone separator consists of an upper cylindrical can with a central outlet tube and a lower conical section with bottom opening (see Fig. 2). An involute inlet section permits the tangential injection of liquid or gaseous mixtures. The spinning centrifugal motion causes denser and coarser particles to gather along the conical walls. Heavier particles precipitate toward the base of the cyclone (the spigot) where the underflow is withdrawn.

The main difference between a purely cyclonic flow and that reproduced inside the NASA sponsored Cool Wall Bidirectional Vortex Combustion Chamber (CW-BVCC) is that the latter exhibits only one outlet section (Fig. 1 versus 2). This

difference is minor because the presence of a secondary outlet does not alter the bulk flow motion. The spigot serves as a collection cavity through which heavy particles may be trickled and filtered out of the mixture. The spigot does not affect the main characteristics of the swirling stream inside the cyclone, especially under high speed conditions for which friction may be discounted.

The purpose of this study is twofold. First, it is to explore both linear and nonlinear solutions of the vorticity transport equation in spherical coordinates under steady, inviscid, incompressible, rotational, and axisymmetric flow conditions. Second, it is to explore possible forms of the solution for the bidirectional vortex that can be used to describe cyclonic motion. In the process, the inviscid vorticity transport equation will be shown to exhibit multiple solutions of which three types will be singled out. These will be considered one-by-one and solved whenever possible.

2. Mathematical model

In seeking an incompressible solution for steady, inviscid, rotational flowfields, it is customary to use the vorticity-stream function approach [29]. Accordingly, one solves $\nabla \times (\mathbf{u} \times \boldsymbol{\omega}) = 0$ and $\boldsymbol{\omega} = \nabla \times \mathbf{u}$. While solutions in Cartesian or cylindrical coordinates are quite common, those in spherical geometry remain a rarity [29, 30]. In the present work, the bidirectional vortex will be formulated using the spatial coordinates (R, ϕ, θ) shown in Fig. 3. Note that in relation to a Cartesian reference frame, ours are defined by $x = R\sin\phi\cos\theta$, $y = R\sin\phi\sin\theta$ and $z = R\cos\phi$.

2.1. Governing equations

In an axisymmetric field in which changes in the θ-directions are null, the equation for continuity reduces to

$$\frac{\partial}{\partial R}(u_R R^2 \sin\phi) + \frac{\partial}{\partial \phi}(u_\phi R \sin\phi) = 0 \tag{2.1}$$

where u_R and u_ϕ are the two components of the velocity vector $\mathbf{u}$. A Stokes stream function $\psi(R, \phi)$ that satisfies Eq. (2.1) can be defined as

$$\frac{\partial \psi}{\partial \phi} = u_R R^2 \sin\phi, \quad \frac{\partial \psi}{\partial R} = -u_\phi R \sin\phi. \tag{2.2}$$

Next, Euler's momentum equation can be reduced to the vorticity transport equation following the usual steps. One gets

$$\nabla \times (\mathbf{u} \times \boldsymbol{\omega}) = 0. \tag{2.3}$$

Equation (2.3) is the steady vorticity transport equation that fulfills the conservation of momentum principle.

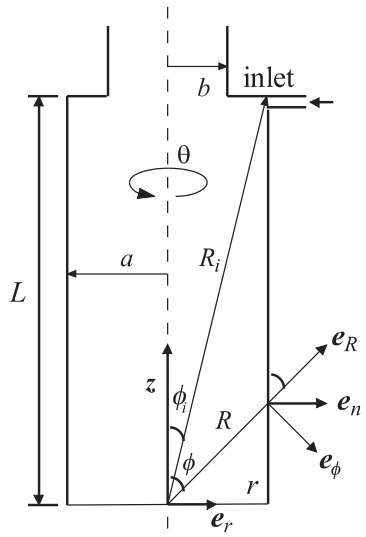

Figure 3. Spherical coordinate system anchored at the chamber's head end.

2.2. Boundary conditions

The boundary conditions for the bidirectional vortex in Fig. 3 are granted by:
(1) Tangential inlet at the wall, namely:

$$Q_i = u_\theta(R_i, \phi_i)A_i = UA_i \tag{2.4}$$

where

$$\phi_i = \tan^{-1}(a/L); \quad R_i = \sqrt{L^2 + a^2}. \tag{2.5}$$

(2) No flow penetration at the head end:

$$u_\phi\left(R, \tfrac{1}{2}\pi\right) = 0. \tag{2.6}$$

(3) No flow crossing of the axis:

$$\phi = 0; \quad u_\phi(R, 0) = 0. \tag{2.7}$$

(4) No flow penetration at the sidewall:

$$R\sin\phi = a; \quad u_n = u_R \sin\phi + u_\phi \cos\phi = 0. \tag{2.8}$$

(5) And, finally, global mass balance; the outflow will match the inflow when:

$$Q_o = Q_i = UA_i, \quad u_z = u_R \cos\phi - u_\phi \sin\phi. \tag{2.9}$$

2.3. Swirl component

In order to capture the behavior of the spin velocity u_θ, it is useful to consider the θ-momentum equation. By virtue of the attendant assumptions, one is left with

$$\left(u_R\frac{\partial}{\partial R}+\frac{u_\phi}{R}\frac{\partial}{\partial\phi}\right)(u_\theta R\sin\phi)=0. \tag{2.10}$$

Since $(\mathbf{u}\cdot\nabla)(u_\theta R\sin\phi)=0$, $u_\theta R\sin\phi=h(\psi)$ must be constant along any streamline. In order to further satisfy Eq (2.4), a free vortex form must be exhibited by the swirling velocity. By restricting our solutions to a constant h, we arrive at

$$u_\theta=UR_i\sin\phi_i/(R\sin\phi). \tag{2.11}$$

The singularity on $R\sin\phi=0$ is a characteristic of inviscid swirling flows [8]. The physics of the problem suggest a boundary layer structure near the chamber axis in the form of a forced core vortex; the latter is known to form due to viscous stresses along the axis of rotation.

2.4 Vorticity-stream function approach

Because u_θ does not appear in the continuity equation, one may invoke the vorticity-stream function approach and replace the remaining components of velocity using

$$u_R=\frac{1}{R^2\sin\phi}\frac{\partial\psi}{\partial\phi},\quad u_\phi=-\frac{1}{R\sin\phi}\frac{\partial\psi}{\partial R}. \tag{2.12}$$

The corresponding vorticity becomes

$$\omega_\theta=\frac{1}{R}\left[\frac{\partial}{\partial R}(Ru_\phi)-\frac{\partial u_R}{\partial\phi}\right];\quad \omega_R=\omega_\phi=0. \tag{2.13}$$

Having realized that the inviscid vorticity gives a single component in the swirl direction, $\omega=\omega_\theta$, one may drop the subscript θ and write

$$\omega=\frac{1}{R}\frac{\partial}{\partial R}(Ru_\phi)-\frac{1}{R}\frac{\partial u_R}{\partial\phi}. \tag{2.14}$$

Substitution into the vorticity transport equation requires evaluating

$$\frac{\partial}{\partial R}\left(\frac{\omega}{R\sin\phi}\frac{\partial\psi}{\partial\phi}\right)-\frac{\partial}{\partial\phi}\left(\frac{\omega}{R\sin\phi}\frac{\partial\psi}{\partial R}\right)=0. \tag{2.15}$$

This will be true when

$$\frac{\omega}{R\sin\phi}=f(\psi). \tag{2.16}$$

A solution of the form $f(\psi)=C\psi^\lambda$ will be sought here although other solutions may exist for which f is not a power of ψ. Three cases can be singled out depending

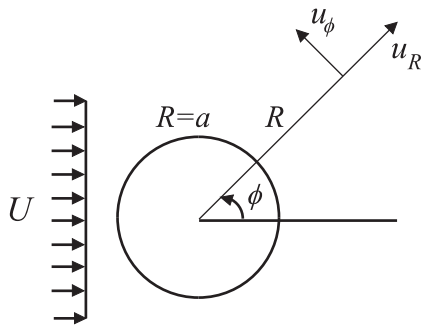

Figure 4. The case of uniform flow past a sphere leading to an inviscid, irrotational solution.

on the exponent λ. Specifically, three types of solutions may be defined viz.

$$\lambda = \begin{cases} 0; & \text{type I} \\ 1; & \text{type II} \\ \text{other}; & \text{type III} \end{cases} . \tag{2.17}$$

3. Possible solutions

The suitability of Eq. (2.17) to describe the bidirectional vortex motion must be tested. We begin by considering the simplest form, namely, the $\lambda = 0$ case.

3.1 Type I solution: potential flow past a sphere

For $\lambda = 0$, one obtains $f(\psi) = C$; the vorticity becomes proportional to $R\sin\phi$. Eq. (2.16) yields $\omega = CR\sin\phi$, which can be readily substituted into Eq. (2.14). The result can be simplified using Eq. (2.2) and put in the form

$$\frac{\partial^2\psi}{\partial R^2} + \frac{\sin\phi}{R^2}\frac{\partial}{\partial\phi}\left(\frac{1}{\sin\phi}\frac{\partial\psi}{\partial\phi}\right) + CR^2\sin^2\phi = 0. \tag{3.1}$$

Assuming a separable solution of the form $\psi = F(R)\sin^2\phi$, it can be shown that

$$R^2F''(R) - 2F(R) = -CR^4 \text{ or } F(R) = C_1R^2 + \frac{C_2}{R} - \frac{C}{10}R^4. \tag{3.2}$$

A type I stream function corresponding to this case is hence unraveled, specifically,

$$\psi = \left(C_1R^2 + \frac{C_2}{R} - \frac{C}{10}R^4\right)\sin^2\phi. \tag{3.3}$$

Unfortunately, this form cannot accommodate the boundary conditions attributed to the bidirectional vortex, given by Eqs. (2.6)–(2.9). Instead, Eq. (3.3) can be

readily adapted to describe the flow conditions associated with a uniform flow past a sphere (c.f. the outer part of Hill's spherical vortex [31]). As illustrated in Fig. 4, this problem exhibits rather simple boundary conditions. In the far field, one has $R \to \infty$, $\psi \to \frac{1}{2}UR^2 \sin^2\phi + \text{const.}$, so that $C = 0$ and $C_1 = \frac{1}{2}U$. The immediate implication is that of an irrotational flow since $\omega = CR\sin\phi = 0$. The corresponding stream function reduces to

$$\psi = \left(\frac{1}{2}UR^2 + \frac{C_2}{R}\right)\sin^2\phi. \tag{3.4}$$

The remaining constant can be obtained from the hard wall boundary condition along the sphere's radius. Given that $\psi(a,\phi) = 0$, one must have $C_2 = -\frac{1}{2}Ua^3$. This leaves us with the familiar solution

$$\psi = \frac{1}{2}UR^2\sin^2\phi\left(1 - \frac{a^3}{R^3}\right) \text{ with } \begin{cases} u_R = 2U\cos\phi(1 - a^3R^{-3}) \\ u_\phi = -\frac{1}{2}U\sin\phi(2 + a^3R^{-3}) \end{cases}. \tag{3.5}$$

This particular result replicates the outer potential flow profile past a sphere; despite being unsuitable for the bidirectional vortex, it is reproduced here in the interest of clarity.

3.2 Type II solution: bidirectional vortex

For $\lambda = 1$, one recovers the classic linear form, $f(\psi) = C^2\psi$. The corresponding vorticity-stream function relation becomes $\omega = C^2\psi R\sin\phi$. Rearward substitution into Eq. (2.14) gives

$$\frac{\partial^2\psi}{\partial R^2} + \frac{1}{R^2}\frac{\partial^2\psi}{\partial\phi^2} - \frac{1}{R^2}\frac{\cos\phi}{\sin\phi}\frac{\partial\psi}{\partial\phi} + C^2\psi R^2\sin^2\phi = 0. \tag{3.6}$$

This is the key equation that needs to be solved for type II behavior.

3.2.1 Separating the vorticity equation

To make progress, we look for similarity solutions of the form $\psi(R,\phi) = \psi(\zeta)$ with the similarity variable $\zeta = \frac{1}{2}C(x^2 + y^2) = \frac{1}{2}CR^2\sin^2\phi$; this requires evaluating

$$\frac{\partial\zeta}{\partial R} = CR\sin^2\phi; \quad \frac{\partial\zeta}{\partial\phi} = CR^2\sin\phi\cos\phi. \tag{3.7}$$

Inserting into Eq. (3.6) yields

$$C\sin^2\phi\psi' + 2C\zeta\sin^2\phi\psi'' - C\sin^2\phi\psi' + 2C\zeta\cos^2\phi\psi'' + 2C\zeta\psi = 0 \tag{3.8}$$

and so

$$2C\zeta(\sin^2\phi + \cos^2\phi)\psi'' + 2\zeta C\psi = 0 \tag{3.9}$$

leading to $\psi'' + \psi = 0$. The standard solution is, of course,

$$\psi = C_1\sin\left(\tfrac{1}{2}CR^2\sin^2\phi\right) + C_2\cos\left(\tfrac{1}{2}CR^2\sin^2\phi\right). \tag{3.10}$$

Equation (3.10) is deceptively simple and can be shown to be unsuitable for the bidirectional vortex. The constants of integration must be permitted to vary in order to capture more complex features of the flow. This will be carried out next.

3.2.2 A more general type II solution

A more general solution for Eq. (3.6) can be pursued in the spirit of Eq. (3.10); for this purpose, one can let

$$\psi = C_1(R,\phi)\sin\left(\tfrac{1}{2}R^2\sin^2\phi\right) + C_2(R,\phi)\cos\left(\tfrac{1}{2}CR^2\sin^2\phi\right). \tag{3.11}$$

This Ansatz may be substituted back into Eq. (3.6); after some algebra, one deduces

$$\begin{aligned}\left\{C\cos\zeta\left[\sin(2\phi)\frac{\partial}{\partial\phi}+2R\sin^2\phi\frac{\partial}{\partial R}\right]+\sin\zeta\left(\frac{\partial^2}{\partial R^2}+\frac{1}{R^2}\frac{\partial^2}{\partial\phi^2}-\frac{\cot\phi}{R^2}\frac{\partial}{\partial\phi}\right)\right\}C_1\\ -\left\{C\sin\zeta\left[\sin(2\phi)\frac{\partial}{\partial\phi}+2R\sin^2\phi\frac{\partial}{\partial R}\right]-\cos\zeta\left(\frac{\partial^2}{\partial R^2}+\frac{1}{R^2}\frac{\partial^2}{\partial\phi^2}-\frac{\cot\phi}{R^2}\frac{\partial}{\partial\phi}\right)\right\}C_2\\ =0.\end{aligned} \tag{3.12}$$

In the interest of clarity, Eq. (3.12) can be written as

$$[C\cos(\zeta)L_1+\sin(\zeta)L_2]C_1-[C\sin(\zeta)L_1-\cos(\zeta)L_2]C_2=0 \tag{3.13}$$

where the operators L_1 and L_2 are defined by

$$\begin{cases} L_1=\sin(2\phi)\dfrac{\partial}{\partial\phi}+2R\sin^2\phi\dfrac{\partial}{\partial R} \\ L_2=\dfrac{\partial^2}{\partial R^2}+\dfrac{1}{R^2}\dfrac{\partial^2}{\partial\phi^2}-\dfrac{\cot\phi}{R^2}\dfrac{\partial}{\partial\phi} \end{cases}. \tag{3.14}$$

The complicating dependence of (3.13) on $\zeta=\frac{1}{2}CR^2\sin^2\phi$ can be averted by restricting our attention to solutions that satisfy

$$\cos(\zeta)(CL_1C_1+L_2C_2)-\sin(\zeta)(L_2C_1-CL_1C_2)=0 \text{ or } \begin{cases} CL_1C_1+L_2C_2=0 \\ L_2C_1-CL_1C_2=0 \end{cases}. \tag{3.15}$$

This coupled set has solutions when

$$(C^2L_1L_1+L_2L_2)C_1=(C^2L_1L_1+L_2L_2)C_2=0. \tag{3.16}$$

Equation (3.16) would, in general, yield interesting solutions of the type assumed in (3.11). However, the resulting fourth-order partial differential equation is rather involved. To make headway, we look for the simpler forms that may be obtained by setting $L_1C_1=L_2C_1=0$ and $L_1C_2=L_2C_2=0$. These translate into

$$\cos\phi\sin\phi\frac{\partial C_1}{\partial\phi}+R\sin^2\phi\frac{\partial^2C_1}{\partial R}=0;\quad \frac{\partial^2C_1}{\partial R^2}+\frac{1}{R^2}\frac{\partial^2C_1}{\partial\phi^2}-\frac{\cot\phi}{R^2}\frac{\partial C_1}{\partial\phi}=0 \tag{3.17}$$

and

$$\cos\phi\sin\phi\frac{\partial C_2}{\partial\phi}+R\sin^2\phi\frac{\partial^2 C_2}{\partial R}=0;\quad \frac{\partial^2 C_2}{\partial R^2}+\frac{1}{R^2}\frac{\partial^2 C_2}{\partial\phi^2}-\frac{\cot\phi}{R^2}\frac{\partial C_2}{\partial\phi}=0. \tag{3.18}$$

Equation (3.17) is linear and can be solved using the method of characteristics. One finds that $C_1 = F(R\cos\phi)$. To determine F, one substitutes the relation $C_1 = F(R\cos\phi)$ back into Eq. (3.17); this operation yields $F''(R\cos\phi) = 0$ or $C_1 = K_1 R\cos\phi + K_2$. Using similar arguments in Eq. (3.18), one finds $C_2 = K_3 R\cos\phi + K_4$. Hence both C_1 and C_2 are linear in z. One form of the type II stream function satisfying Eq. (3.6) becomes

$$\psi = (K_1 R\cos\phi + K_2)\sin\zeta + (K_3 R\cos\phi + K_4)\cos\zeta. \tag{3.19}$$

3.2.3. Axisymmetric behavior

Based on Eqs. (2.12) and (3.19), one can re-evaluate the velocity components

$$\begin{aligned} u_R = &\Big[\left(-K_3 + CK_2 R\cos\phi + CK_1 R^2\cos^2\phi\right)\cos\zeta \\ &-\left(K_1 + CK_4 R\cos\phi + CK_3 R^2\cos^2\phi\right)\sin\zeta\Big]/R \end{aligned} \tag{3.20}$$

$$\begin{aligned} u_\phi = -\Big\{&[K_3\cot\phi + CR(K_2 + K_1 R\cos\phi)\sin\phi]\cos\zeta \\ &-[K_1\cot\phi - C(K_4 + K_3 R\cos\phi)\sin\phi]\sin\zeta\Big\}/R. \end{aligned} \tag{3.21}$$

Axisymmetry demands that K_3 and K_4 be zero lest the component of the velocity be unbounded along the axis. At the outset, the solution appropriate of axisymmetric flows reduces to

$$\psi = (K_1 R\cos\phi + K_2)\sin\zeta \tag{3.22}$$

with the companion velocities being

$$\begin{cases} u_R = [CR\cos\phi(K_1 R\cos\phi + K_2)\cos\zeta - K_1\sin\zeta]/R \\ u_\phi = -[CR\sin\phi(K_1 R\cos\phi + K_2)\cos\zeta + K_1\cot\phi\sin\zeta]/R \end{cases}. \tag{3.23}$$

Equation (3.23) represents the type II class of solutions found here for an axisymmetric flowfield.

3.2.4. Specific case: cylindrical bidirectional vortex

A cylindrical cyclone or a CWBVCC chamber may be modeled as a cylindrical tube of length L and radius a; the head end may be considered impermeable (due to the corresponding small volumetric flux associated with the underflow in a cyclone or the fuel injected in the CWBVCC); the aft end may be assumed to be partially open to a straight nozzle of radius b. A sketch of the chamber is given in Fig. 3 where R, ϕ and θ are used to guide spherical variations. Note that the origin of the spherical coordinate system is placed at the center of the chamber

head end; alternatively, r and z are used to represent the cylindrical radial and axial coordinates in a coincident reference frame. The fraction of the radius that is open to flow may be defined by $\beta = b/a$ and the chamber's aspect ratio by $l = L/a$.

Excluding axisymmetry (which is already satisfied) the remaining physical conditions described in Eqs. (2.6)–(2.9) may now be applied to Eq. (3.23). Firstly, the state of no flow across the head end requires that $u_\phi\left(R, \frac{1}{2}\pi\right) = 0$; hence

$$u_\phi = -CC_1K_2\cos\left(\tfrac{1}{2}CR^2\right) = 0. \tag{3.24}$$

This is true when $K_2 = 0$ or $\psi = K_1R\cos\phi\sin\zeta$. One is left with

$$\begin{cases} u_R = K_1(CR^2\cos^2\phi\cos\zeta - \sin\zeta)/R \\ u_\phi = -K_1(CR^2\cos\phi\sin\phi\cos\zeta + \cot\phi\sin\zeta)/R \end{cases}. \tag{3.25}$$

Secondly, one can enforce the no flow across the sidewall where the radius a remains invariant. Accordingly, the component of the velocity normal to the surface must vanish along $R\sin\phi = a$. Based on geometric considerations, the component of velocity u_n normal to the sidewall may be evaluated from

$$u_n = u_R\sin\phi + u_\phi\cos\phi, \quad R = a\csc\phi \tag{3.26}$$

where

$$u_R = K_1\sin\phi\left[Ca\cot^2\phi\cos\left(\tfrac{1}{2}Ca^2\right) - \sin\left(\tfrac{1}{2}Ca^2\right)/a\right] \tag{3.27}$$

and

$$u_\phi = -K_1\sin\phi\left[Ca\cot\phi\cos\left(\tfrac{1}{2}Ca^2\right) + \cot\phi\sin\left(\tfrac{1}{2}Ca^2\right)/a\right]. \tag{3.28}$$

Equation (3.26) becomes

$$u_n = -(K_1/a)\sin\left(\tfrac{1}{2}Ca^2\right) \tag{3.29}$$

The no flow across the sidewall requires that $u_n = 0$ or $\sin\left(\frac{1}{2}Ca^2\right) = 0$. This condition precipitates

$$C = 2n\pi/a^2, \quad n = 1, 2\ldots. \tag{3.30}$$

Hence, $\psi = K_1R\cos\phi\sin(n\pi a^{-2}R^2\sin^2\phi)$. For a single pass bidirectional motion, one must set $n = 1$ such that

$$\psi = K_1R\cos\phi\sin(\pi a^{-2}R^2\sin^2\phi) \tag{3.31}$$

$$\begin{cases} u_R = K_1[2\pi a^{-2}R^2\cos^2\phi\cos(\pi a^{-2}R^2\sin\phi) - \sin(\pi a^{-2}R^2\sin^2\phi)]/R \\ u_\phi = -K_1[2\pi a^{-2}R^2\cos\phi\sin\phi\cos(\pi a^{-2}R^2\sin^2\phi) + \cot\phi\sin(\pi a^{-2}R^2\sin^2\phi)]/R \end{cases}. \tag{3.32}$$

The last constant K_1 may be deduced from global mass balance. In Fig. 3, it can be seen that, for flow across a cylindrical face, the axial velocity consists of the combination

$$u_z = u_R\cos\phi - u_\phi\sin\phi \tag{3.33}$$

such that

$$u_z = \frac{K_1}{R}\left[2\pi a^{-2}R^2\cos^2\phi\cos(\pi a^{-2}R^2\sin^2\phi) - \sin(\pi a^{-2}R^2\sin^2\phi)\right]\cos\phi + \frac{K_1}{R}\left[2\pi a^{-2}R^2\cos\phi\sin\phi\cos(\pi a^{-2}R^2\sin^2\phi) + \cot\phi\sin(\pi a^{-2}R^2\sin^2\phi)\right]\sin\phi. \tag{3.34}$$

This, in turn, simplifies into

$$u_z = 2\pi a^{-2}K_1 R\cos\phi\cos(\pi a^{-2}R^2\sin^2\phi) = 2\pi a^{-2}K_1 z\cos(\pi a^{-2}r^2). \tag{3.35}$$

The global mass balance across the outlet requires that $Q_o = Q_i = UA_i$; hence

$$Q_o = \int_0^b u_z(r,L)2\pi r dr = \int_0^b 4\pi^2 a^{-2}K_1 L\cos(\pi a^{-2}r^2)r dr = 2\pi K_1 L\sin(\pi a^{-2}b^2). \tag{3.36}$$

For this to hold, the last constant must be

$$K_1 = \frac{UA_i}{2\pi L\sin(\pi a^{-2}b^2)}. \tag{3.37}$$

The bidirectional vortex specific to a cylindrical chamber is now at hand. One has

$$\psi = \frac{UA_i R\cos\phi\sin(\pi a^{-2}R^2\sin^2\phi)}{2\pi L\sin(\pi a^{-2}b^2)} \tag{3.38}$$

with the spherical components

$$u_R = \frac{UA_i}{2\pi RL\sin(\pi a^{-2}b^2)}\left[2\pi a^{-2}R^2\cos^2\phi\cos(\pi a^{-2}R^2\sin^2\phi) - \sin(\pi a^{-2}R^2\sin^2\phi)\right] \tag{3.39}$$

and

$$u_\phi = \frac{-UA_i}{2\pi RL\sin(\pi a^{-2}b^2)} \cdot\left[2\pi a^{-2}R^2\cos\phi\sin\phi\cos(\pi a^{-2}R^2\sin^2\phi) + \cot\phi\sin(\pi a^{-2}R^2\sin^2\phi)\right]. \tag{3.40}$$

This completes the bidirectional vortex representation in spherical coordinates.

3.3. Type III solution: nonlinear behavior

For $f(\psi) = C^2\psi^\lambda$, $\forall\lambda \neq (0,1)$, a nonlinear relation ensues between the vorticity and stream function. This is perhaps the most interesting case as one must reconsider

$$\frac{\partial^2\psi}{\partial R^2} + \frac{\sin\phi}{R^2}\frac{\partial}{\partial\phi}\left(\frac{1}{\sin\phi}\frac{\partial\psi}{\partial\phi}\right) + f(\psi)R^2\sin^2\phi = 0 \tag{3.41}$$

with f exhibiting the nonlinear form

$$f(\psi) = C\psi^\lambda \tag{3.42}$$

for some C and λ. If we now assume ψ of the form

$$\psi(R,\phi) = F(R)G(\phi) \tag{3.43}$$

we get

$$\frac{d^2F(R)}{dR^2}G(\phi) + CF^{\lambda}(R)G^{\lambda}(\phi)R^2\sin\phi + \frac{F(R)\sin\phi}{R^2}\frac{d}{d\phi}\left[\frac{1}{\sin\phi}\frac{dG(\phi)}{d\phi}\right] = 0 \tag{3.44}$$

or

$$\frac{R^2}{F(R)}\frac{d^2F(R)}{dR^2} + CF^{\lambda-1}G^{\lambda-1}R^4\sin^2\phi + \frac{\sin\phi}{G(\phi)}\frac{d}{d\phi}\left[\frac{1}{\sin\phi}\frac{dG(\phi)}{d\phi}\right] = 0. \tag{3.45}$$

By applying the transformation $F(R) = H(R)\sqrt{R}$, we are left with

$$\frac{R^2}{F(R)}\frac{d^2F(R)}{dR^2} = -\frac{1}{4} + R\frac{H'}{H} + R^2\frac{H''}{H}. \tag{3.46}$$

In seeking a separable solution, one must equate Eq. (3.46) to a constant; if this constant is chosen to be $\mu^2 - \frac{1}{4}$, Euler's differential equation is recovered, namely

$$RH' + R^2H'' = \mu^2 H. \tag{3.47}$$

As usual, the solution exhibits the form

$$H(R) = AR^{\mu} + BR^{-\mu}. \tag{3.48}$$

With this information, the rest of Eq. (3.45) becomes independent of R. As we look for solutions that are regular at $R = 0$, we pick

$$H(R) = R^{\mu} \tag{3.49}$$

and so

$$\mu^2 - \frac{1}{4} + \frac{\sin\phi}{G(\phi)}\frac{d}{d\phi}\left[\frac{1}{\sin\phi}\frac{dG(\phi)}{d\phi}\right] + CR^{(\mu+\frac{1}{2})(\lambda-1)+4}G^{\lambda-1}(\phi)\sin^2\phi = 0. \tag{3.50}$$

Clearly, Eq. (3.50) can be made independent of R by choosing

$$\left(\mu + \tfrac{1}{2}\right)(\lambda - 1) + 4 = 0 \tag{3.51}$$

or

$$\mu = 4/(1-\lambda) - \tfrac{1}{2}. \tag{3.52}$$

This choice turns Eq. (3.50) into

$$\sin\frac{d}{d\phi}\left[\frac{1}{\sin\phi}\frac{dG(\phi)}{d\phi}\right] + CG^{\lambda}(\phi)\sin^2\phi + \left(\mu^2 - \frac{1}{4}\right)G(\phi) = 0. \tag{3.53}$$

The resulting ODE has to be solved subject to the periodicity condition needed for a physically meaningful problem, specifically, $G(0) = G(2\pi)$ and $G'(0) = G'(2\pi)$. This condition places restrictions on the possible choices of C and λ.

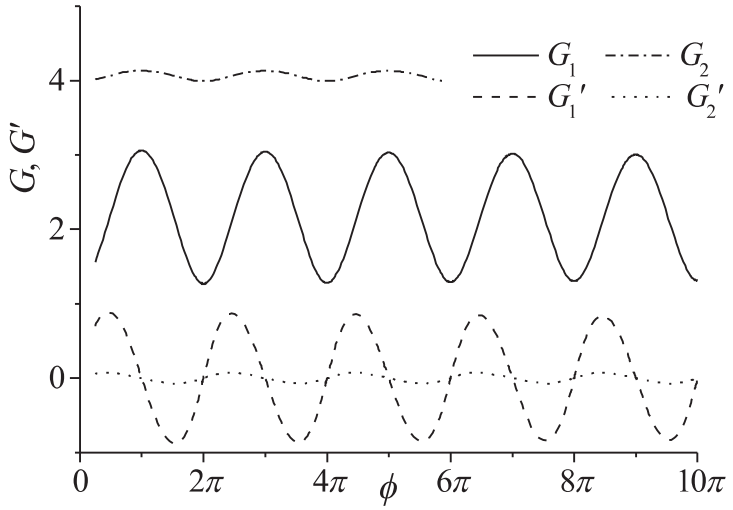

Figure 5. Sample plot of the periodic results of the nonlinear type III solution for the specific case of $\lambda = -3$ and $C = 1$. The two case illustrate the solution multiplicity with different initial conditions.

Equation (3.53) is nonlinear because, as it can be seen from Eq. (3.51), any choice of λ may be possible except for $\lambda = 1$. Using primes to denote differentiation with respect to ϕ, Eq. (3.53) can be written as

$$G'' - \cot\phi G' + CG^{\lambda}\sin^2\phi + 4(\lambda+3)(\lambda-1)^{-2}G = 0. \tag{3.54}$$

Multiple solutions may thus be obtained but those that are meaningful must satisfy the periodicity condition. For example, using $\lambda = -3$ ($\mu = \frac{1}{2}$), and $C = -1$, Eq. (3.54) becomes

$$G''(\phi) - \cot\phi G'(\phi) + G^{-3}(\phi)\sin^2\phi = 0. \tag{3.55}$$

This can be solved numerically to obtain multiple periodic solutions. The resulting behavior is illustrated in Fig. 5 where it is solved using two sets of initial guesses. These are

$$\begin{cases} G_1(\pi/4) = 1.558501, & G_1'(\pi/4) = 0.7000145 \\ G_2(\pi/4) = 4.016863, & G_2'(\pi/4) = 0.05790198 \end{cases}. \tag{3.56}$$

Note that, for each set, a candidate solution is obtained.

Interestingly, for the special case of $\lambda = -3$ ($\mu = 1/2$), an exact analytical solution can be obtained for arbitrary C. This can be seen by re-examining Eq. (3.53) which now becomes

$$\frac{1}{\sin\phi}\frac{d}{d\phi}\left(\frac{1}{\sin\phi}\frac{dG}{d\phi}\right) + CG^{-3} = 0. \tag{3.57}$$

By letting $\chi = \cos\phi$ and $G(\phi) = C^{1/4}g(\chi)$, Eq. (3.57) simplifies into the equation for planetary motion in a central force field, namely, $g'' + g^{-3} = 0$ (primes are

associated with χ). This simple result can be multiplied by g' and integrated to produce

$$\tfrac{1}{2}(g')^2 - \tfrac{1}{2}g^{-2} = \text{ constant } = \tfrac{1}{2}K_1 \tag{3.58}$$

or $g' = \pm\sqrt{K_1 + g^{-2}}$. A second integration attempt furnishes

$$\pm \int^{g} \frac{K_1 \xi}{\sqrt{1 + K_1 \xi^2}} d\xi = \pm\sqrt{1 + K_1 g^2} = K_1 \chi + K_2. \tag{3.59}$$

Hence, $1 + K_1 g^2 = (K_1\chi + K_2)^2$, or $g(\chi) = \pm\sqrt{[(K_1\chi + K_2)^2 - 1]/K_1}$. Finally, a type III solution emerges from

$$G(\phi) = \pm C^{1/4} \left[\frac{(K_1 \cos\phi + K_2)^2 - 1}{K_1} \right]^{1/2} \tag{3.60}$$

and so, in combination with Eqs. (3.49) and (3.43), one collects

$$\psi(R, \phi) = \pm C^{1/4} R \left[\frac{(K_1 \cos\phi + K_2)^2 - 1}{K_1} \right]^{1/2} \tag{3.61}$$

with

$$\begin{cases} u_R = \mp \dfrac{C^{\frac{1}{4}} K_1^{1/2} (K_1 \cos\phi + K_2)}{R\left[(K_1 \cos\phi + K_2)^2 - 1\right]^{\frac{1}{2}}} \\ u_\phi = \mp \dfrac{C^{\frac{1}{4}} \left[(K_1 \cos\phi + K_2)^2 - 1\right]^{\frac{1}{2}}}{K_1^{1/2} R \sin\phi} \end{cases} . \tag{3.62}$$

This particular profile cannot be made to satisfy the boundary conditions implied in the bidirectional vortex. However, it may find useful application elsewhere.

4. Comparison to earlier work

To verify that the bidirectional vortex is valid inside a cylinder, it may be compared to the solution obtained in earlier work [32]. In order to do so, one can employ the coordinate transformations $R\cos\phi = z$ and $R\sin\phi = r$. The corresponding velocities are related vis-à-vis

$$\begin{cases} u_r = u_R \sin\phi + u_\phi \cos\phi \\ u_z = u_R \cos\phi - u_\phi \sin\phi \end{cases} . \tag{4.1}$$

Transformation of the spherical solution yields

$$u_r = \frac{-K_1}{R\sin\phi} \sin(\pi a^{-2} R^2 \sin^2\phi) \tag{4.2}$$

which, from Eq. (3.37), simplifies into

$$u_r = \frac{-U A_i \sin(\pi a^{-2} R^2 \sin^2\phi)}{2\pi L R \sin\phi \sin(\pi a^{-2} b^2)} = \frac{-U A_i \sin(\pi a^{-2} r^2)}{2\pi L r \sin(\pi \beta^2)} \tag{4.3}$$

where $\beta = b/a$. Similarly, one finds

$$u_z = 2\pi a^{-2} K_1 z \cos(\pi a^{-2} r^2) = \frac{U A_i z \cos(\pi a^{-2} r^2)}{L a^2 \sin(\pi a^{-2} b^2)} \tag{4.4}$$

and, from Eq. (2.11),

$$u_\theta = \frac{U R_i \sin\phi_i}{R \sin\phi} = \frac{U R_i \sin\phi_i}{r} = \frac{Ua}{r}. \tag{4.5}$$

To render Eqs. (4.3)–(4.5) dimensionless, one may use the overbar to denote dimensionless quantities:

$$\bar{r} = \frac{r}{a}, \quad \bar{z} = \frac{z}{a}, \quad \bar{u}_r = \frac{u_r}{U}, \quad \bar{u}_\theta = \frac{u_\theta}{U}, \quad \bar{u}_z = \frac{u_z}{U}, \quad \frac{A_i}{a^2} = \sigma^{-1}. \tag{4.6}$$

The resulting normalized velocities become

$$\begin{cases} \bar{u}_r = \dfrac{-\sin(\pi \bar{r}^2)}{2\pi\sigma l \bar{r} \sin(\pi\beta^2)} = -\dfrac{\kappa}{\bar{r}} \dfrac{\sin(\pi \bar{r}^2)}{\sin(\pi\beta^2)}; \quad \bar{u}_\theta = \dfrac{1}{\bar{r}} \\ \bar{u}_z = \dfrac{\bar{z} \cos(\pi \bar{r}^2)}{\sigma l \sin(\pi\beta^2)} = 2\pi\kappa\bar{z} \dfrac{\cos(\pi \bar{r}^2)}{\sin(\pi\beta^2)} \end{cases} \tag{4.7}$$

where $\kappa = (2\pi\sigma l)^{-1}$ is the tangential inlet parameter. It should be noted that, in order for the outflow radius to match that of the nozzle inlet, the outflow radius should be $b = a/\sqrt{2}$ or $\beta = 1/\sqrt{2}$. Under these idealized conditions, the bidirectional vortex collapses into

$$\bar{u}_r = -\frac{\kappa}{\bar{r}} \sin(\pi \bar{r}^2), \quad \bar{u}_\theta = \frac{1}{\bar{r}}, \quad \bar{u}_z = 2\pi\kappa\bar{z} \cos(\pi \bar{r}^2). \tag{4.8}$$

Equation (4.8) is identical to the non-dimensional solution obtained in [32]. This confirms the validity of our spherical solution. For a numerical verification, it may be instructive to present a sample of the results obtained by an independent group of investigators who employed a computational fluid dynamics code [26, 33]. This code specializes in solving the coupled, three-dimensional Navier–Stokes equations for a chemically reactive, multi-phase and compressible flow.

In this simulation, the nominal mesh consisted of 184×35 axial and radial grid cells. This included 12 grid cells in the axial direction to resolve the injection area. The grid cell spacing in both the radial and axial directions was non-uniform to permit better grid concentration near the walls and near regions of higher flow gradients.

Using an aspect ratio of $l = 3.43$, $A_i = 10^{-3}$ m^2, $U = 260$ m s^{-1}, $UA_i = 0.26$ m^3 s^{-1}, $\rho = 2.24$ kg m^{-3}, $\mu = 9.6 \times 10^{-5}$ kg m^{-1} s^{-1}, $a = 0.0673$ m and, therefore, a Reynolds number of $Re = \rho U a/\mu = 4 \times 10^5$, the vector field computed numerically is shown in Fig. 6a. Using a similar geometry and flow intensity, the vector plot produced from (3.70) is displayed in Fig. 6b for a nozzle outlet ratio corresponding to $\beta = 1/\sqrt{2}$.

Despite the disparity in the governing equations and assumptions used in the present work vis-à-vis those employed in the numerical simulations, it is interesting

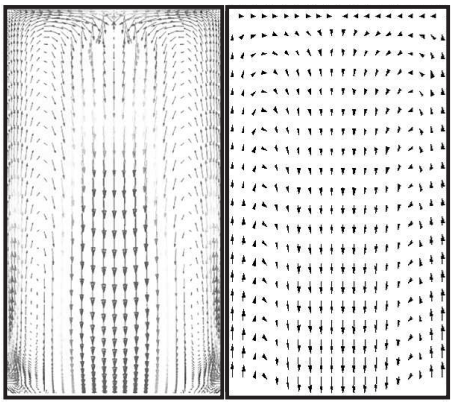

Figure 6. Vector plots comparing some numerical simulations of the bidirectional vortex with those obtained analytically.

to note the favorable agreement between theory and computation. In both cases, the flow enters at the base, travels upwardly, and then turns sharply near the head end; after reversing direction at the chamber head end, the flow returns to the base area where it exits through the open nozzle section. Based on the numerical solution, the thin boundary layer near the chamber wall appears too small to be discerned graphically. The small size of this layer supports the idea of an inviscid fluid; this idealization seems to hold well near the wall.

Along the corners of the head end and base sections, the gradual flow curvature that is captured by the Navier–Stokes solver is due to viscous effects that elude the present analytical model. Nonetheless, both analytical and numerical solutions confirm the existence of cross flow between the outer and inner vortex regions along the length of the chamber. They also confirm the presence of the so-called mantle separating the outer and inner vortex tubes.

In addition to this independent investigation, it may be worth mentioning that three-dimensional numerical simulations were carried out by Fang, Majdalani and Chiaverini under both cold [16] and reactive flow conditions [34]. Therein, favorable comparisons with (4.8) were made, with better agreement being reported in the cold flow investigation.

5. Concluding remarks

In this paper we have examined several solutions in the context of steady, axisymmetric, incompressible, and inviscid vortex motion in spherical coordinates. In addition to the quest for generalizations of the nonlinear vorticity transport

equation, particular attention has been given to the specific solution that will satisfy the physical conditions associated with a single pass, bidirectional vortex. By identifying different classes of solutions, the work furnishes procedural steps that may be applied to other geometric shapes, with the conical cyclone being one such example.

To verify the analysis, the type I solution is shown to reproduce the outer potential flow past a sphere, one of the few spherical solutions available in the literature. However, it is the type II solution that is able to accommodate the bidirectional vortex in a straight cylinder. As the latter is obtained in inviscid form, it unravels the free vortex motion that is known to affect the bulk flow away from the core [8]. Near the chamber axis, viscous stresses appreciate as transition to a forced vortex progresses [35]. The treatment of attendant structures is hoped to be accomplished in later work. So will be the discussion of other solutions with single or multiple flow passes. In the interim, incorporation of viscous terms will be needed in the forced vortex analysis to capture the core motion and to resolve the boundary layers adjacent to the endwall and sidewall. Finally, the new type III class of solutions, engendered from the nonlinear vorticity transport equation, is found to exhibit both numerical and exact outcomes. It is hoped that their analysis will promote additional research in those physical settings that are more manageable in spherical geometry.

Acknowledgments

This project was sponsored by Grant No. CMS-0353518 of the National Science Foundation. The first author acknowledges valuable discussions with Dr. Martin J. Chiaverini, Lead Propulsion Engineer of Orbital Technologies Corporation (ORBITEC), Madison, Wisconsin. His support for this project is most gratefully appreciated.

References

[1] A. J. ter Linden, Investigations into cyclone dust collectors, *Proc. Inst. Mech. Engrs* **160** (1949), 233–251.

[2] D. F. Kelsall, A study of motion of solid particles in a hydraulic cyclone, *Trans. Inst. Chem. Engrs* **30** (1952), 87–103.

[3] J. L. Smith, An experimental study of the vortex in the cyclone separator, *ASME J. Basic Engng -Trans. ASME* (1962), 602–608.

[4] J. L. Smith, An analysis of the vortex flow in the cyclone separator, *ASME J. Basic Engng -Trans. ASME* (1962), 609–618.

[5] F. J. Fontein and C. Dijksman, *Recent Developments in Mineral Dressing*, Institution of Mining and Metallurgy, London 1953.

[6] M. I. G. Bloor and D. B. Ingham, Theoretical investigation of the flow in a conical hydrocyclone, *Trans. Inst. Chem. Engrs* **51** (1973), 36–41.

[7] M. I. G. Bloor and D. B. Ingham, On the use of Pohlhausen method in three dimensional boundary layers, *J. Appl. Math. Phys. (ZAMP)* **28** (1977), 289–299.
[8] M. I. G. Bloor and D. B. Ingham, The flow in industrial cyclones, *J. Fluid Mech.* **178** (1987), 507–519.
[9] R. F. Reydon and W. H. Gauvin, Theoretical and experimental studies of confined vortex flow, *Canad. J. Chem. Engng* **59** (1981), 14–23.
[10] G. H. Vatistas, S. Lin and C. K. Kwok, Theoretical and experimental studies on vortex chamber flows, *AIAA J.* **24** (4) (1986), 635–642.
[11] G. H. Vatistas, S. Lin and C. K. Kwok, Reverse flow radius in vortex chambers, *AIAA J.* **24** (11) (1986), 1872–1873.
[12] G. H. Vatistas, Tangential velocity and static pressure distributions in vortex chambers, *AIAA J.* **25** (8) (1987), 1139–1140.
[13] K. T. Hsieh and R. K. Rajamani, Mathematical model of the hydrocyclone based on physics of fluid flow, *AICHE J.* **37** (5) (1991), 735–746.
[14] A. J. Hoekstra, J. J. Derksen and H. E. A. Van den Akker, An experimental and numerical study of turbulent swirling flow in gas cyclones, *Chem. Engng Sci.* **54** (1999), 2055–2065.
[15] J. J. Derksen and H. E. A. Van den Akker, Simulation of vortex core precession in a reverse-flow cyclone, *AICHE J.* **46** (7) (2000), 1317–1331.
[16] D. Fang, J. Majdalani and M. J. Chiaverini, Simulation of the cold-wall swirl driven combustion chamber, *AIAA Paper* 2003–5055, 2003.
[17] J. Smagorinsky, General circulation experiments with the primitive equations: 1. The basic experiment, *Monthly Weather Review* **91** (1963), 99.
[18] D. G. Lilley, Swirl flows in combustion: A review, *AIAA J.* **15** (8) (1977), 1063–1078.
[19] F. Boysan, W. H. Ayers and J. Swithenbank, A fundamental mathematical modelling approach to cyclone design, *Institute of Chemical Engineers* **60** (1982), 222.
[20] A. K. Gupta, D. G. Lilley and N. Syred, *Swirl Flows*, Abacus, London, UK 1984.
[21] L. X. Zhou and S. L. Soo, Gas-solids flow and collection of solids in a cyclone separator, *Power Technology* **63** (1990), 45.
[22] T. Dyakowski and R. A. Williams, Modelling turbulent flow within a small-Diameter hydrocyclone, *Chem. Engng Sci.* **48** (1993), 1143.
[23] P. A. Yazdabadi, A. J. Griffiths and N. Syred, Characterization of the PVC phenomena in the exhaust of a cyclone dust seperator, *Exper. Fluids* **17** (1994), 84–95.
[24] S. Elgobashi, On predicting particle-laden turbulent flows, *Appl. Sci. Res.* **52** (1994), 309.
[25] A. J. Griffiths, P. A. Yazdabadi and N. Sred, Alternative eddy shedding set up by the nonaxisymmetric recirculation zone at the exhaust of a cyclone dust separator, *Journal of Fluids Engineering* **120** (1998), 193.
[26] M. J. Chiaverini, M. J. Malecki, J. A. Sauer and W. H. Knuth, Vortex combustion chamber development for future liquid rocket engine applications, *AIAA Paper* 2002–2149, 2002.
[27] M. J. Chiaverini, M. J. Malecki, J. A. Sauer, W. H. Knuth and C. D. Hall, Final report on cold-wall vortex combustion chamber-a phase I SBIR project, report OTC-GS0107-01-1, Orbital Technological Corporation, 2001. NASA Contact No. NAS8-01073 Report.
[28] M. J. Chiaverini, M. M. Malecki, J. A. Sauer, W. H. Knuth and C. D. Hall, Testing and evaluation of vortex combustion chamber for liquid rocket engines, *JANNAF Paper*, 2002.
[29] F. M. White, *Viscous Fluid Flow*, McGraw-Hill, New York 1991.
[30] H. Schlichting, *Boundary-Layer Theory*, 7th ed., McGraw-Hill, New York 1979.
[31] M. J. M. Hill, On a spherical vortex, *Phil. Trans. R. Soc. Lond. A* **185** (1894), 213–245.
[32] A. B. Vyas, J. Majdalani and M. J. Chiaverini, The bidirectional vortex. Part 1: an exact inviscid solution, *AIAA Paper* 2003–5052, 2003.
[33] M. J. Chiaverini, M. J. Malecki, J. A. Sauer, W. H. Knuth and J. Majdalani, Vortex thrust chamber testing and analysis for O2-H2 propulsion applications, *AIAA Paper* 2003–4473, 2003.
[34] D. Fang, J. Majdalani and M. J. Chiaverini, Hot flow model of the vortex cold wall liquid rocket, *AIAA Paper* 2004–3676, 2004.

[35] A. B. Vyas, J. Majdalani and M. J. Chiaverini, The bidirectional vortex. Part 2: viscous core corrections, *AIAA Paper* 2003–5053, 2003.

Joseph Majdalani
Jack D. Whitfield Professor of High Speed Flows
Department of Mechanical, Aerospace and Biomedical Engineering
University of Tennessee Space Institute
Tullahoma, TN 37388
USA

Sjoerd W. Rienstra
Department of Mathematics and Computing Science
Eindhoven University of Technology
NL-5600 MB Eindhoven
Netherlands

(Received: May 26, 2005; revised: February 17, 2006)

Published Online First: September 6, 2006


To access this journal online:
http://www.birkhauser.ch